Electron-scale Turbulence Spectra and Plasma Thermal Transport Responding to Continuous ExB Shear Ramping-up in a Spherical Tokamak

Y. Ren[1], W. Guttenfelder[1], S. M. Kaye[1], E. Mazzucato[1], K. C. Lee[2], C. W. Domier[2]

[1]Princeton Plasma Physics Laboratory, Princeton, NJ 08543

[2]University of California at Davis, Davis, CA 95616

E-mail contact of main author: yren@pppl.gov

Abstract. Microturbulence is considered to be a major candidate in driving anomalous transport in fusion plasmas, and the equilibrium ExB shear generated by externally driven flow can be a powerful tool to control microturbulence in future fusion devices such as FNSF and ITER. Here we present the first observation of the change in electron-scale turbulence wavenumber spectrum (measured by a high-k scattering system) and thermal transport responding to continuous ExB shear ramping-up in an NSTX center-stack limited and NBI-heated L-mode plasma. It is found that while linear stability analysis shows that the maximum ETG mode linear growth rate far exceeds the observed ExB shearing rate in the measurement region of the high-k scattering system, the unstable ITG modes are susceptible to ExB shear stabilization. We observed that as the ExB shearing rate is continuously ramped up in the high-k measurement region, the ratio between the ExB shearing rate and the maximum ITG mode growth rate continuously increases (from about 0.2 to 0.7) and the maximum power of the measured electron-scale turbulence wavenumber spectra decreases. Meanwhile, both the electron and ion thermal transports are also reduced as long as MHD activities are not important. These observations are found to be consistent with ExB shear stabilization of ion-scale turbulence.

1. Introduction

Microturbulence is considered to be a major candidate in driving anomalous transport in fusion plasmas [1], and the Ion Temperature Gradient (ITG) mode [2], Trapped Electron Mode (TEM) [3], Electron Temperature Gradient (ETG) mode [4] and micro-tearing mode [5-7] are well-known instabilities which could drive micro-turbulence. One important aspect of the controlled magnetic fusion research is to understand the operational micro-instabilities in fusion plasma and their operational regimes and thus to control them in future fusion devices, e.g. Fusion Nuclear Science Facility (FNSF) [8] and ITER. An important tool for controlling microturbulence in these devices is the equilibrium ExB shear generated by externally driven (or intrinsically generated) plasma flow [9]. It was pointed out that ExB shear affects microturbulence and associated turbulent transport both linearly and nonlinearly: change mode stability, e.g. enhance damping by coupling to stable modes; change the relative phase between fluctuation quantities, e.g. density fluctuation and radial velocity fluctuations; reduce fluctuation amplitude. The most physical way to determine the effect of ExB shear on turbulence is to compare ExB shearing rate, $\omega_{E\times B}$, with turbulence decorrelation rate as pointed out in Ref. [10]. However, the turbulence decorrelation rate is usually unknown, and a rule of thumb is that turbulence should be significantly stabilized by ExB shear when the Hahm-Burrell ExB shearing rate [10], $\omega_{E\times B,HB}$, is larger than the maximum linear growth rate of a particular instability, γ_{max} [9]. A quantitative numerical study of ExB shear effects on turbulence and transport was reported in Ref. [11], where extensive linear and nonlinear gyrokinetic simulations were used to determine the amount of ExB shearing rate needed for quenching a specific kind of plasma turbulence. In particular, a quenching threshold for the ion-scale turbulence (ITG/TEM) is found to be $\omega_{E\times B,WM}/\gamma_{max} \approx 1.41(A/3)^{0.6}/(\kappa/1.5)$, where $\omega_{E\times B,WM}$ is the Waltz-Miller ExB shearing rate [12], $\gamma_{max}$is the maximum linear growth rate for a particular instability, A is the local aspect ratio and κ is the local elongation. Indeed, experiments have shown that increase in ExB shear is correlated with the

formation of H-mode edge transport and internal barriers and reduction in ion-scale turbulence [13,14]. However, we note that in these cases, the ExB shear mainly comes from pressure gradient rather than from plasma rotation. On the other hand, spherical tokamaks (STs) with tangential neutral beam heating typically have strong toroidal flow with Mach number approaching 1, and ExB shear can be dominated by the contribution from plasma rotation. Thus ion-scale turbulence is expected to be stabilized by ExB shear, which is supported by the observed neoclassical level of ion thermal transport in STs [15,16]. Furthermore, ExB shear was also shown to suppress electron-scale turbulence when the ExB shearing rate is comparable to the maximum ETG linear growth rate [17], where the turbulence spectrum was measured by a high-k scattering system [18] on the National Spherical Torus eXperiment (NSTX) [19]. However, the change in spectral shape was not explored in Ref. [17] since only a single k measurement was available due to limitations in the scattering scheme, and most importantly correlation with transport was not investigated.

Here, with much improved scattering schemes of this high-k scattering system, we present the first experimental observation of a progressive change in electron-scale turbulence k spectrum and thermal confinement at the core-edge transition region of a set of NSTX NBI-heated L-mode plasmas (r/a~0.66-0.78), as the ExB shearing rate is continuously increased due to plasma toroidal velocity increase from Neutral Beam Injection (NBI). We observed that as the ExB shearing rate is continuously increased, the ratio between the ExB shearing rate and the maximum ITG mode growth rate continuously increases and the maximum power of the measured electron-scale turbulence wavenumber spectra decreases. Meanwhile, both the electron and ion thermal transports are also reduced as long as MHD activities are not important. These observations are consistent with that some of the observed electron-scale turbulence is nonlinearly driven by ITG turbulence and its power decreases as ITG turbulence is progressively suppressed by ExB shear.

2. Experimental Apparatus

Figure 1 plots the scattering configuration of the high-k scattering system [18] used in the study presented in this paper, including the probe beam and scattered beam trajectories calculated using a ray tracing code. The five receiving channels cover a wavenumber range of $5\ cm^{-1} \lesssim k_{\perp} \lesssim 30\ cm^{-1}$ with a resolution of about 1 cm^{-1}, and five heterodyne receivers allow us to distinguish the wave propagation direction for each different wavenumber. Heterodyne detection is carried out for each channel, which allows us to distinguish wave propagation direction. The power response of each receiving channel was calibrated with a solid-state microwave source with known output power. The frequency response of the scattering system is about 5 MHz. A radial resolution of $\Delta R \approx \pm$ 2 cm, determined by the 1/e half width of the microwave beam power, is the unique feature of the scattering system. This is made possible by the tangential launching scheme along with the large toroidal curvature of NSTX due to its low aspect ratio, which leads to a scattering volume much smaller than that from the

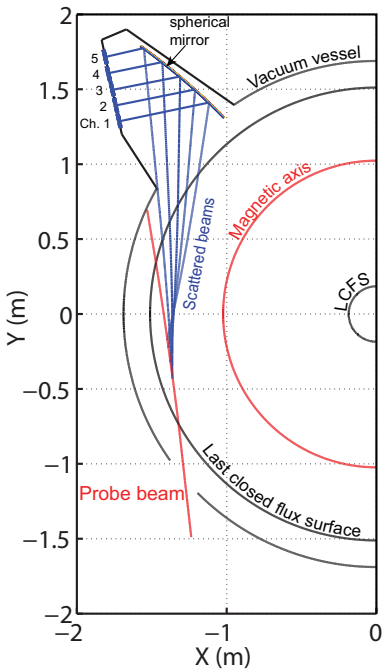

Figure 1 Schematic of the scattering configuration of the high-k scattering system used in the study presented in this paper. The probe beam and scattered beam trajectories are calculated using a ray-tracing code. Scattered light is reflected and focused by a spherical mirror onto five collection windows.

overlapping of the probe and scattering beams [20]. This fine radial resolution allowed us to study the dependence of locally measured turbulence on local equilibrium quantities, e.g. L_{T_e} [21] (electron temperature scale length), L_{n_e} [22,23] (electron density scale length), collisionality [23], q (safety factor), and $\hat{s}$ (magnetic shear) [24]. Recent improvements in scattering scheme have significantly reduced stray radiation, which made it possible to obtain scattering signals from all five channels simultaneously, compared to at most three channels previously [25]. Newly implemented remote control capability allows between-shot adjustment of launching and receiving optics, which made it possible to optimize scattering configuration according to realized plasma equilibria. We note that due to the tangential launching scheme employed (see Fig. 1), the scattering system measures mostly radial wavenumber, k_r, and finite but smaller poloidal wavenumber, k_θ, e.g. a range of $k_r\rho_s \sim$ 5-13 and a range of $k_\theta\rho_s \sim$ 2-4 for the experiments presented in this paper. We note that as shown in Fig. 1, the scattered beam to channel 5 is partially blocked by the vacuum vessel and thus is not used in the following analysis.

3. Results

Observations on continuous ExB shear ramping-up were made in a set of center-stack limited and NBI-heated L-mode plasmas. These plasmas have a toroidal field of 5.5 kG, a plasma current of 900 kA and a two-phase NBI with the first 2 MW NBI pulse from about 100 ms to 200 ms and the second 2 MW NBI pulse from about 350 ms to the end of discharges. During the second phase of NBI, plasma continuously spins up, which leads to a simultaneous increase in the ExB shearing rate in the outer half of the plasma (r/a $\gtrsim$ 0.5). Here in this paper, we present the observations from shot 141716 for which we have done extensive analysis. In this shot, the second 2 MW NBI pulse is re-injected from 335 ms after a first injection from 90 ms to 230 ms (see Fig. 2). The line integrated electron density shows continuous but slow increase through the shown time window. The low frequency Mirnov signal shows that no large MHD activity is present at beginning of the second NBI pulse (from 330 ms to 450 ms) and that an n=1 mode starts to grow at about t=450 ms and saturates at about t=470 ms. With the presence of the 2 MW NBI pulses, ion temperature and plasma toroidal velocity are measured with a charge exchange recombination spectroscopy (CHERS) diagnostic [26] and magnetic field pitch angle is measured by a Motional Stark Effect (MSE) diagnostic [27]. Electron temperature and density are measured with Multi-point Thomson Scattering (MPTS) [28]. Plasma equilibrium is obtained using LRDFIT (LR circuit model with Data FITting capabilities) [29] equilibrium reconstructions constrained by magnetic pitch angle measurements from the MSE diagnostic [27] and electron temperature iso-surfaces. The stored energy (calculated using a time dependent tokamak transport and data analysis code (TRANSP) [30]) is shown to increase continuously in the beginning of the second NBI pulse and saturates at about the same time as the n=1 MHD mode, which may not be coincident. It

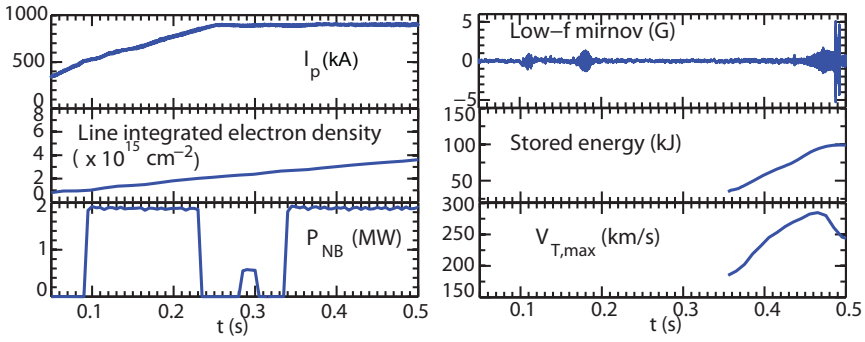

Figure 2 An overview of shot 141716 with time traces of plasma current, linear integrated electron density, neutral beam power P_{NB}, low-f magnetic fluctuation, stored energy and maximum plasma toroidal flow velocity.

is also clear that the maximum plasma toroidal velocity, $V_{T,max}$, also increases steadily after the second NBI pulse is initiated, indicating a continuous increase in ExB shear. We note that since we will be concentrating on the second pulse of NBI and CHERS measurements are not available the period between the two NBI pulses, stored energy and $V_{T,max}$ are only shown for the time period of the second NBI pulse.

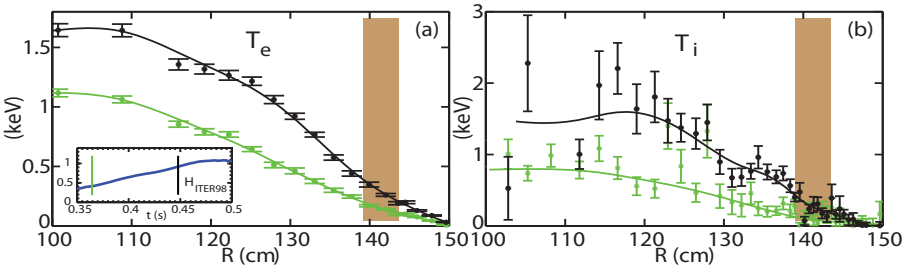

Figure 3 (a) Radial profiles of electron temperature at t=364 and 448 ms. (d) Radial profiles of ion temperature at t=364 and 448 ms. The shaded regions in both panels denote the measuring of the high-k scattering system. Note that the insert in (a) shows the time trace of H_{ITER98} and the two vertical lines denotes the time points used for (a) and (b).

The electron and ion temperature, T_e and T_i, radial profiles are plotted in Fig. 3(a) and (b) at t=364 ms and at t=448 ms (corresponding to two exact MPTS time points). The high-k measurement region, the overall radial region covered by all channels with the center of scattering location separated by $\lesssim$1 cm, is denoted by the shaded region in the figure from about R=139 to 144 cm (r/a~0.66-0.78). The H_{ITER98} time trace in the insert in Fig. 3(a) shows about a factor of 2 increase in H_{ITER98} from t=350 ms to 500, and we note that this increase coincides with the increase of plasma toroidal flow velocity shown in Fig. 1. We can see that both the maximum T_e and T_i increase by 50-100% as H_{ITER98} (and toroidal flow velocity) increases, and both T_e and T_i gradients also increase in the high-k measurement region. On the other hand, we would like to point out that the gradient scale lengths remain relatively constant. We note that although the energy confinement of this L-mode plasma reaches that of the H-mode plasmas in conventional tokamaks, no formation of an energy transport barrier has been observed, and as we will show later, thermal transport is reduced significantly in the outer half of the plasmas which is consistent with the increased ExB shear there.

In Fig. 4, we present how measured turbulence changes as plasma spins up. The upper panels Fig. 4 show the spectrograms of the scattered signals from t=350 ms to 500 ms (during which the plasma is spinning up), where the two exact MPTS time points, i.e. t=364 and 448 ms, are denoted by two colored lines in each panel. The lower panels show the frequency spectra at the above two time points for each of the four high-k channels. The wavenumbers measured by the four channels correspond to $k_\perp \rho_s$ of 8-10, 6-8, 4-6 and 2-4 from channel 1 to 4 at t=364 ms. At t=448 ms, because of the increase in T_e and density gradient, ρ_s and the wavenumber measured by each channel become larger, corresponding to $k_\perp \rho_s$ of 13-15, 10-12, 7-9 and 4-6 from channel 1 to 4 respectively. For each channel, the signal from collective scattering of microwave by electron density fluctuations manifests as a spectral peak at negative frequencies, which corresponds to wave propagation in the ion diamagnetic drift direction in the laboratory frame (Lab frame). However, each channel has a Doppler frequency shift [$f_{Doppler}=k_T V_T/2\pi$, k_T is the toroidal wavenumber from ray tracing and V_T is the plasma toroidal flow velocity from CHERS measurement] denoted by vertical lines in the lower panels of Fig. 4. After subtracting the Doppler shift, channels 1, 2, 3 and 4 show that the spectral peaks of the scattered signals fall in the electron diamagnetic direction which is on the right hand side of the vertical lines (For clarity, only $f_{Doppler}$ at t=364 ms is shown but conclusion is the same for t=448 ms), and thus the wave propagation direction is in the electron direction. We also note that the large symmetric central peaks at f=0 are due to the spurious reflections of the probing microwave beam. Large frequency separation of the

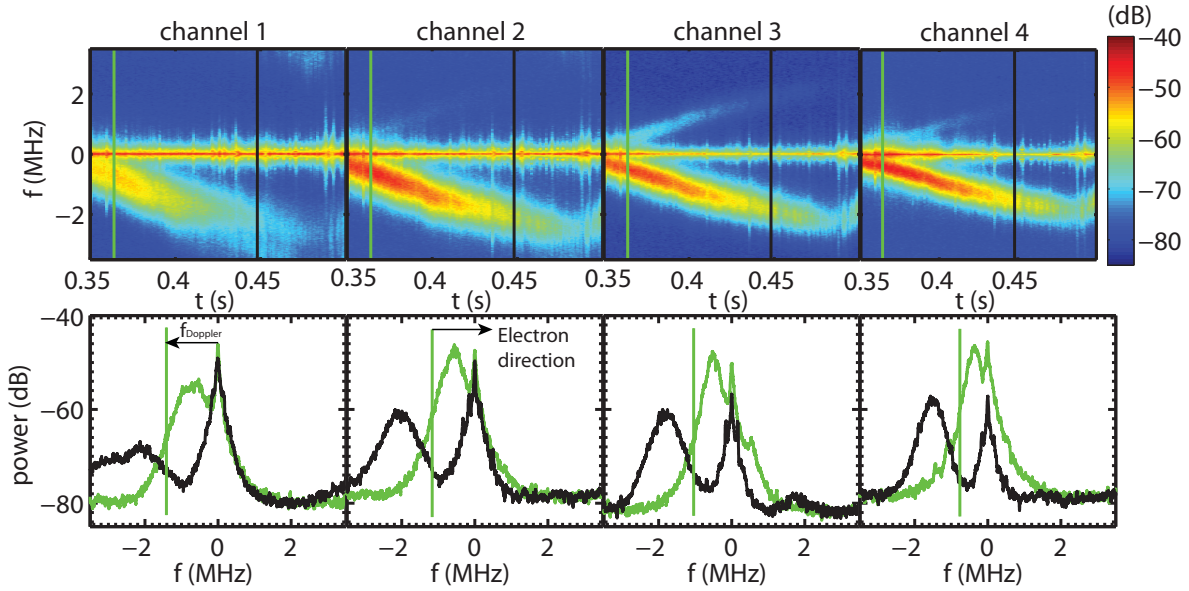

Figure 4 Upper panels: The spectrograms of four high-k channels during the second NBI phase; Lower panels: The frequency spectra at the two exact MPTS time points (the same as in Fig. 3) for four high-k channels. The two colored lines in the upper panels denote time points used for plotting the lower panels with the same color coding and the vertical lines in the lower panels denote the Doppler frequencies, $f_{Doppler}=k_T V_T/2\pi$, for different channels at t=364 ms (Note that for clarity, only $f_{Doppler}$ at t=448 ms is not shown). The electron direction is on the ride hand side of the vertical lines in the lower panels, as shown for channel 2.

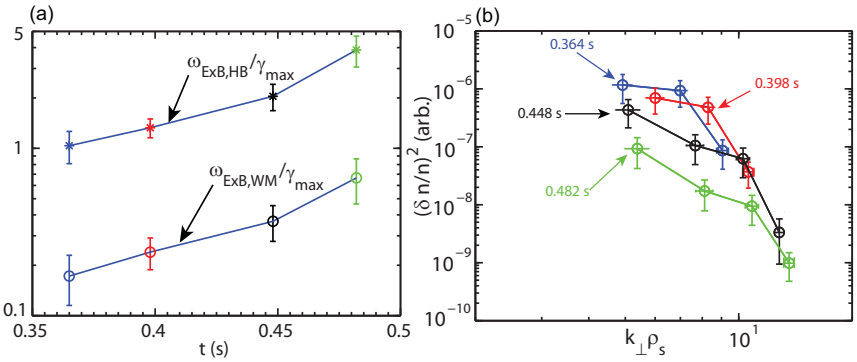

Figure 5 (a) The ratio between the ExB shear rate and the maximum linear growth rate for ITG modes (both the Hahm-Burrell ($\omega_{E\times B,HB}$) and Waltz-Miller ($\omega_{E\times B,WM}$) ExB shearing rates are shown); (b) $k_\perp$ spectra in arbitrary unit at the 4 time points shown in (a).

scattering signals from the central peaks ensures accurate measurements of scattered microwave power. From Fig. 4, it can be immediately seen that the measured fluctuations in all channels show continuous increase in Lab-frame fluctuation frequency, consistent with a Doppler shift frequency resulting from plasma spin-up. Furthermore, it is also clear that the fluctuation intensity denoted by color in the spectrograms shows gradual decrease as the Lab-frame fluctuation frequency increases (a more quantitative evaluation of the decrease can be seen in the lower panels).

To model ExB shear effect on microturbulence, nonlinear gyrokinetic simulations are needed. However, here we use linear stability analysis to provide some initial assessment of the ExB shear effect in the experiment, motivated by the studies on ExB shearing rate and linear growth rate reported in Refs 9 and 11. Here, the ExB shearing rate is calculated with radial electric field from TRANSP [30]. In Fig. 5 (a), $\omega_{E\times B}/\gamma_{max}$ averaged in the high-k measurement region is plotted as a function of time (Note that both $\omega_{E\times B,HB}$ and $\omega_{E\times B,WM}$ are used and they differ by about a factor of 5), and γ_{max} is the maximum linear growth rate for the most unstable ion-scale instability (ITG modes) calculated with the GS2 code [31]. We note that the gradual increase of $\omega_{E\times B}/\gamma_{max}$ from t=364 to 448 ms is due to the increase of $\omega_{E\times B}$, while the faster increase of $\omega_{E\times B}/\gamma_{max}$ after t= 448 ms is due to both the increase of

$\omega_{E\times B}$ and decrease of γ_{max}. Figure 5(b) shows the measured $k_\perp$ spectra at time points used in Fig. 5(a). From t=364 to 398 ms, the measured maximum spectral power (at $k_\perp\rho_s \approx 5$) decreases by about 40% while $\omega_{E\times B,WM}/\gamma_{max}$ increases from about 0.17 to 0.24. Meanwhile, the spectral power at larger wavenumbers ($k_\perp\rho_s \gtrsim 8$) has about a factor of 2 increase, and it appears that the slope of the spectra (at $k_\perp\rho_s \gtrsim 7$ for t=364 ms and at $k_\perp\rho_s \gtrsim 8$ for t=398 ms) is preserved. Larger decreases, about 60-80%, in spectral power at $k_\perp\rho_s \lesssim 10$ occur while $\omega_{E\times B,WM}/\gamma_{max}$ approaches 0.4 at t=448 ms and 0.7 at t=482 ms. We note that from t=398 to 448 ms the k spectra seem to preserve the shape and power at $k_\perp\rho_s \gtrsim 10$, but at t=482 ms the spectral power at $k_\perp\rho_s \gtrsim 10$ also starts to drop. This overall decrease in spectral power with the large $\omega_{E\times B,WM}/\gamma_{max}$ (~0.7) at t=482 ms is consistent with being close to the quenching threshold $\omega_{E\times B,WM} \approx (1.1-1.2)\gamma_{max}$ calculated using the quenching rule in Ref. [11] with the local A≈1.9-2.1 and the local $\kappa \approx 1.5$. Since the maximum ETG growth rate in the high-k measurement region, $\gamma_{max} \sim 10 - 20C_s/a$ (C_s is the sound speed and a is the plasma minor radius), is much larger than the experimental ExB shearing rate [$(0.1-0.4)C_s/a$], ETG turbulence is unlikely to be affected by the experimental amount of ExB shear. However, as we have shown in Fig. 5 (b), electron-scale turbulence indeed decreases as ExB shear is increased, and this motivates us to speculate that some of the observed electron-scale turbulence is nonlinearly driven by the ion-scale turbulence and its power decreases as the ion-scale turbulence is progressively suppressed by the ExB shear.

Having shown the variation in electron-scale turbulence responding to the equilibrium change in the high-k measurement region, here we present the accompany changes in plasma thermal transport together with the profile change in ExB shearing rate. The transport analysis was carried out with TRANSP [30]. Figure 6(a) and (b) plot the radial profiles of ExB shearing rate using both the Waltz-Miller definition [12] and the Hahm-Burrell definition [10]. It is clear that the ExB shearing rate increases are at outer half of the plasma, r≳130 cm (r/a≳0.5), from t=364 to 448 ms. We note that the ExB shearing rate increase in this time period is correlated with the increase in $V_{T,max}$ as shown in Fig. 2. From t=448 to 482 ms, the region of ExB shearing rate increase moves further out to r≳139 cm (r/a≳0.7). It can be seen from Fig. 2 that $V_{T,max}$ saturates and starts to decrease in this time period, and the increase in ExB shearing rate is due to change in the toroidal flow profile, most likely due to momentum transport from the n=1 MHD mode. We also note that the ExB shearing rates have large radial variation especially at t=448

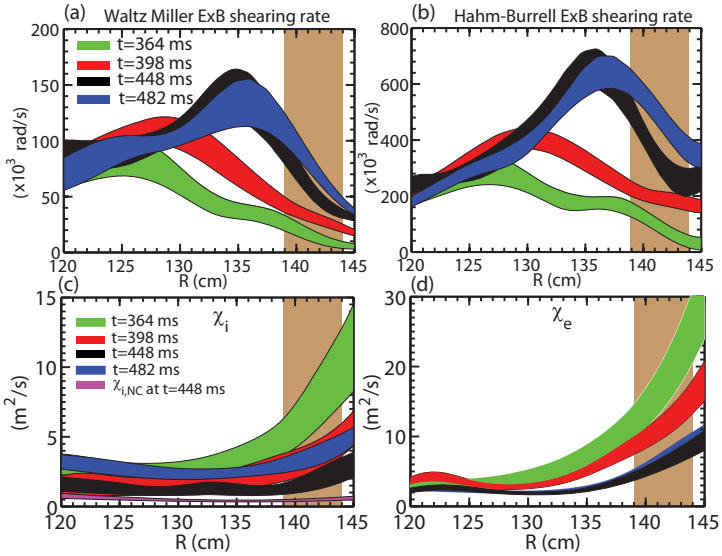

Figure 6 (a) Radial profiles of the Waltz-Miller ExB shearing rate at t=364 (green), 398 (red), 448 (black) and 482 (blue) ms; (b) Radial profiles of the Hahm-Burrell ExB shearing rate at the same time points and with the same color coding as in (a); (c) Radial profiles of ion thermal diffusivity, χ_i, at at the same time points and with the same color coding as in (a) and radial profile of neoclassical ion thermal diffusivity at t=448 ms (magenta); (d) Radial profiles of ion thermal diffusivity, χ_e, at the same time points with the same color coding as in (a). Note that the horizontal width of the colored regions denotes the experimental uncertainty. The width of rectangular shaded region denotes the high-k measurement region.

and 482 ms, i.e. $\gtrsim$ a factor of 2 variation in the high-k measurement region and $\gtrsim$ a factor of 3 from R≈135 to 145 cm, which indicates that global effects may be important in modeling plasma thermal transport, e.g. with gyrokinetic simulations.

The ion and electron thermal diffusivity profiles at the times of interest used are plotted in Fig. 6 (c) and (d). (We note that the uncertainty in χ_i and χ_e in Fig. 6 (c) and (d) is mainly due to uncertainties in ohmic heating and measured kinetic profiles). We can immediately see that the largest decrease in both χ_i and χ_e occurs at $R \gtrsim 130\,cm$ $(r/a \gtrsim 0.5)$, which coincides well with where the ExB shear varies most in the experiment. Figure 6 also shows that from t=364 to 398 ms, χ_i decreases by about 50% and $\chi_e$decreases by about 35% in the high-k measurement region, and a decrease in χ_i and χ_e by about 50% occurs from t=398 to 448 ms, which correlates well with the changes in $\omega_{E\times B,WM}/\gamma_{max}$ shown in Fig. 5(a), i.e. about 40% increase from t=364 to 398 ms and about 50% from t=398 to 448 ms. χ_i is always anomalous since at its smallest at t=448 ms, it only approaches to a factor of about 2-3 of the ion neo-classical thermal diffusivity, $\chi_{i,NC}$, which is consistent with the ion-scale turbulence not being completely quenched as indicated by the comparison with the quenching threshold previously. We also point out that χ_i becomes larger and χ_e remains essentially the same from t=448 to 482 ms, even though $\omega_{E\times B}/\gamma_{max}$ is almost doubled. As we have pointed out (see Fig. 2), an n=1 MHD mode starts to grow at about t=450 ms and saturates at about t=470 ms. Thus it is likely that this MHD mode can enhance both ion and electron thermal transport at t=482 ms in addition to microturbulence.

4. Discussions and Summary

In this paper, we have presented the first observation of the change in electron-scale turbulence wavenumber spectrum and thermal transport responding to continuous ExB shear ramping-up in an NSTX center-stack limited and NBI-heated L-mode plasma, where the global energy confinement continues to increase and reaches the H-mode confinement of conventional tokamaks in a time period of plasma spin-up. During the same time period, the frequency spectra of electron-scale turbulence measured by the microwave scattering system clearly shows an almost linear increase in fluctuation frequency and a decrease in fluctuation power as the plasma toroidal flow speed increases. The former is consistent with the increase in Doppler frequency due to plasma spin-up, and the later indicates an interplay between sheared flow and plasma turbulence.

Although to investigate the effect of ExB shear on plasma turbulence nonlinear simulations are needed, in this paper we took an initial approach by comparing ExB shearing rate and maximum growth rates of unstable ITG and ETG modes (calculated by GS2 code [31]), and this approach was shown to reasonably represent the nonlinear ExB shear stabilization effect on turbulence [11]. We found that while linear stability analysis shows that the maximum ETG mode linear growth rate far exceeds the observed ExB shearing rate in the measurement region of the high-k scattering system, the unstable ITG modes are susceptible to ExB shear stabilization. As the ExB shearing rate is continuously ramped up in the high-k measurement region, the ratio between the ExB shearing rate and the maximum ITG mode growth rate continuously increases (from about 0.2 to 0.7) but does not reach the quenching threshold predicted by using the result from Ref. 11, and at the same time the maximum power of the measured electron-scale turbulence wavenumber spectra decreases. However, we have pointed out that the observed ExB shearing rate is close to ITG growth rate but is much smaller than ETG growth rate, and thus a nonlinear coupling between ion and electron scale is needed to explain the observed reduction in electron-scale turbulence. It could be that some of the electron-scale turbulence is a result of nonlinear cascade from ITG turbulence or ETG turbulence is nonlinearly excited by ITG turbulence, and once ITG turbulence is stabilized by

ExB shear, the resulting electron-scale turbulence is also reduced. Multi-scale nonlinear gyrokinetic simulations are planned to fully investigate this nonlinear coupling.

Furthermore, both the electron and ion thermal transports are found to decrease in the outer half of the plasma coinciding with where ExB shear changes most, when MHD activities are small. The fact that the measured ion thermal diffusivity, at its minimum, is still 2-3 times the neoclassical value is consistent with that the ITG turbulence is stabilized but not completely quenched by ExB shear. Local and global nonlinear simulations are being used to quantitatively characterize the ExB shear effect on ITG turbulence and results will be reported in future papers. In addition, $\chi_e > \chi_i$ as shown in Fig.6 shows that electrons are the dominant transport channel, and thus ETG turbulence may be contributing to the thermal transport as ITG does. This observation further supports our plan of carrying out multi-scale nonlinear gyrokinetic simulations.

Acknowledgements: This work was supported by U.S. Dept. of Energy contracts No. DE-AC02-09CH11466, No. DE-FG03-95ER54295, and No. DE-FG03-99ER54518.

References:

[1] W. Tang, Nuclear Fusion 18, 1089 (1978).
[2] B. Coppi and F. Pegoraro, Nuclear Fusion 17, 969 (1977).
[3] B. Kadomtsev and O. Pogutse, Nuclear Fusion 11, 67 (1971).
[4] Y. C. Lee et al., Physics of Fluids 30, 1331 (1987).
[5] R. D. Hazeltine and H. R. Strauss, Phys. Rev. Lett. 37, 102 (1976).
[6] J. F. Drake et al., Phys. Rev. Lett. 44, 994 (1980).
[7] W. Guttenfelder et al., Phys. Plasmas 19, 022506 (2012)
[8] J. E. Menard et al., Nuclear Fusion 51, 103014 (2011).
[9] K. H. Burrell, Physics of Plasmas 4, 1499 (1997).
[10] T. S. Hahm and K. H. Burrell, Phys. Plasmas 2, 1648 (1995).
[11] J. E. Kinsey et al., Physics of Plasmas 14, 102306 (2007).
[12] R. E. Waltz and R. L. Miller, Physics of Plasmas 6, 4265 (1999).
[13] C. P. Ritz et al., Phys. Rev. Lett. 65, 2543 (1990).
[14] E. Mazzucato et al., Phys. Rev. Lett. 77, 3145 (1996).
[15] S. M. Kaye et al., Nucl. Fusion 47, 499 (2007).
[16] A. R. Field et al., Proc. 20th Int'l. Atomic Energy Agency Fusion Energy Conference, Vilamoura, Portugal, 1-6 November 2004, CD-ROM file EX/P2-11 (IAEA, Vienna, 2004).
[17] D. R. Smith et al., Phys. Rev. Lett. 102, 225005 (2009).
[18] D. R. Smith et al., Rev. Sci. Instrum. 79, 123501 (2008).
[19] M. Ono et al., Nuclear Fusion 40, 557 (2000).
[20] E. Mazzucato, Phys. Plasmas 10, 753 (2003).
[21] E. Mazzucato et al., Phys. Rev. Lett. 101, 075001 (2008).
[22] Y. Ren et al., Phys. Rev. Lett. 106, 165005 (2011).
[23] Y. Ren et al., Physics of Plasmas 19, 056125 (2012).
[24] H. Y. Yuh et al., Phys. Rev. Lett. 106, 055003 (2011).
[25] E. Mazzucato et al., Nuclear Fusion 49, 055001 (2009).
[26] R. E. Bell, Rev. Sci. Instrum. 77, 10E902 (2006).
[27] F. M. Levinton et al., Phys. Plasmas 14, 056119 (2007).
[28] B. P. LeBlanc et al., Rev. Sci. Instrum. 74, 1659 (2003).
[29] J. E. Menard et al., Phys. Rev. Lett. 97, 095002 (2006).
[30] R. J. Hawryluk, Physics of Plasma Close to Thermonuclear Conditions (Pergamon, New York, 1981).
[31] M. Kotschenreuther et al., Comp. Phys. Comm. 88, 128 (1995).